

Ultrafast and On-Demand Oil/Water Separation Membrane System Based on Conducting Polymer Nanotip Arrays

Zhengao Wang,[▽] Peng Yu,[▽] Jiajia Zhou, Jingwen Liao, Lei Zhou, Heying Ran, Jingxia Zhai, Jun Xing, Guoxin Tan, Zhengnan Zhou, Yangfan Li, Chengyun Ning,^{*} and Yahong Zhou^{*}

Cite This: *Nano Lett.* 2020, 20, 4895–4900

Read Online

ACCESS |

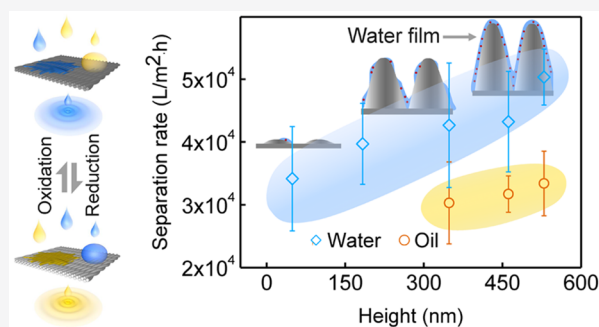
Metrics & More

Article Recommendations

Supporting Information

ABSTRACT: Ultrafast oil/water separation based on tunable superwettability switch remains a big challenge. Here, inspired by the ultrafast water transport mechanism in *sarracenia*, we develop a micro/nanostructured porous membrane with conducting polymer nanotip arrays through the surface-initiated polymerizations. By modulating the height (ranging from 49–529 nm) and redox states of nanotips, a smart reversible superwettability switch is facile to obtain with contact angles of water/oil arranging from 161° to about 0°. Besides, liquid transport speed was accelerated more than 1.5 times by increasing the nanotip length. The water flux could reach up to 50326 L m⁻² h⁻¹ (1000 times that of a typical industrial ultrafiltration membrane). This is attributed to the stable and continuous water film along the nanotips, which provide a lubrication layer, leading to an increase of permeability. This work provides significant insights into macro/nanostructured membrane design for smart separation, blood lipid filtration, and smart nanoreactors with high permeability.

KEYWORDS: conducting polymer nanotip arrays, tunable wettability switch, ultrafast, oil/water separation membrane system



Industrial oily wastewater and frequent crude oil spills usually contain toxic chemicals that can cause catastrophic damage to ecosystems and people's health. Therefore, it is very urgent to develop a method for selective separating large amounts of organic pollutants or water from the mixture.^{1–4} The traditional techniques for oil/water separation such as air flotation, gravity separation combined with skimming, oil-absorbing materials, coagulation, and flocculation are limited by low separation efficiency, energy cost, complex separation instruments, and further treatment necessary.^{5–8} These methods cannot selectively separate oil or water. Recently, the stimuli-responsive membrane with special superwetting, which were applied for the controlled oil/water separation, has attracted abundant attention.^{9–11} Due to their selective affinities toward water and oil, i.e., superhydrophobic–superoleophilic, superhydrophilic–superoleophobic, or superhydrophilic–underwater superoleophobic properties, such materials can separate only one of the oil–water mixtures while selectively repelling the other phase to achieve controlled oil/water separation.^{12–14} Feng et al. fabricated a superoleophilic and superhydrophobic mesh film to separate oil and water from mixture.¹ Up to now, two typical functional materials, underwater superoleophobic surfaces and superhydrophobic/superoleophilic surfaces, have been successfully designed and employed in smart oil/water separation.¹⁵ Furthermore, the synergistic effect between surface architecture and chemistry can further enhance the superwetting

behavior, leading to improved separation efficiency.¹⁶ However, reversible ultrafast oil/water separation remains a challenge.

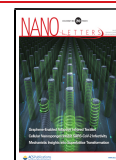
To achieve high permeability, researchers generally designed the membrane by decreasing the thickness of the separating layer.¹⁷ For example, ultrathin single-walled carbon nanotube network films achieved oil/water separation with ultrahigh flux.¹⁸ Although a dramatic increase in permeability, the mechanical property of these membranes may be significantly reduced, which restricted the practical and commercial applications.² The biological system may give us some inspiration on how to reduce the internal resistance of the membrane.^{19,20} For example, Chen and Jiang et al. found that a liquid thin film in *sarracenia* could improve the water transport speed.²¹ Therefore, designing membranes capable of forming a stable liquid film could settle the permeability limit.

Herein, we designed a novel micro/nanostructured porous membrane with conducting polymer nanotip arrays through the surface-initiated polymerizations. The superwetting switch and ultrafast selective oil/water separation of the functional

Received: March 1, 2020

Revised: June 14, 2020

Published: June 22, 2020



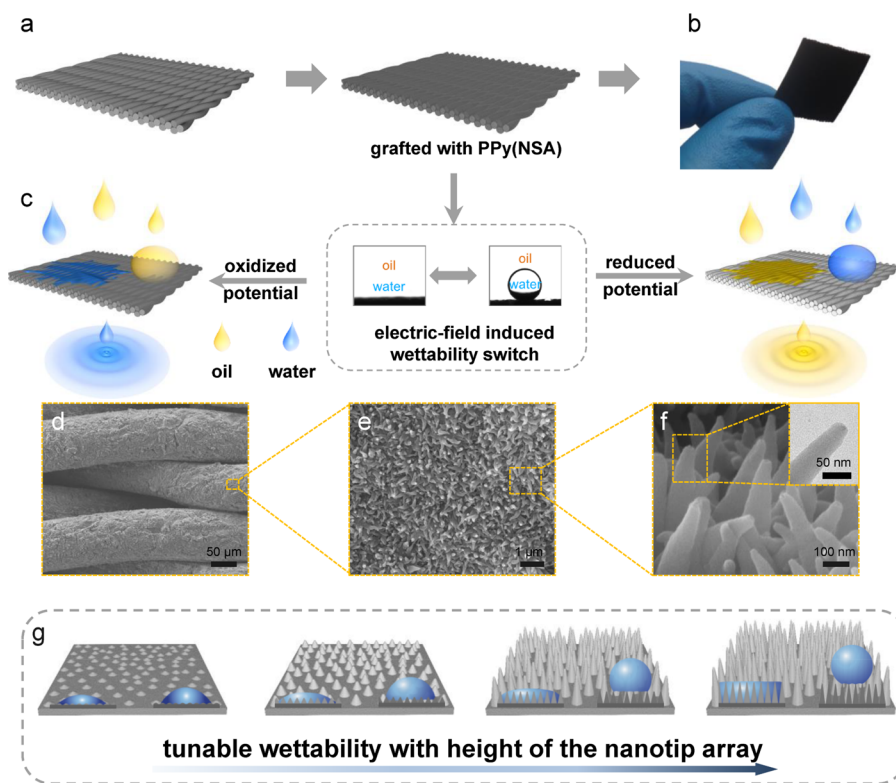


Figure 1. Schematic of fabrication, oil/water separation, and wettability switch of micro/nanostructured porous membrane with conducting polymer nanotips. (a) The PPy nanotips are grafted on the titanium mesh through electrochemical deposition. (b) Optical images of the membrane are shown. (c) Due to the reversible wettability switch, the functional membrane could realize ultrafast selective oil/water separation. (d)–(f) Field emission scanning electron microscopy (FE-SEM) images of the membrane are shown. Inset in (f): transmission electron microscopy (TEM) of single nanotips. (g) The height of the nanotips enhance the reversible wettability switch.

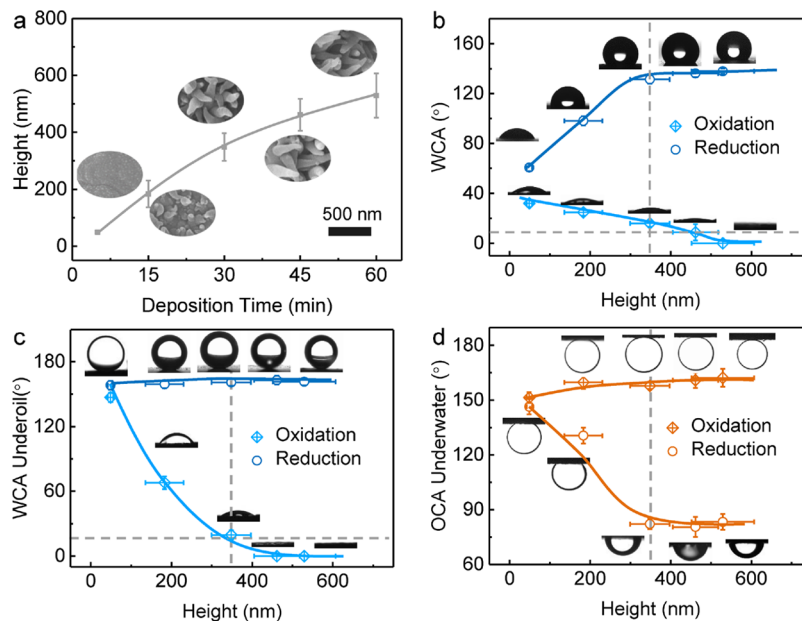


Figure 2. Wettability switch behavior with different heights of nanotips and different chemical states. (a) The height of the nanotips was precisely regulated by controlling the deposition time. And the height of the nanotips and the chemical state dominate the water contact angle (WCA) of the membrane in air (b) and in oil (c) and the oil contact angle (OCA) in water (d). The vertical gray dotted line shows the critical height was about 348 nm, where the interface performed superwetting in air or oil.

membrane are facile to realize by applying a weak electric field. A stable and continuous liquid film prefers to be formed along the nanotips, promoting liquid transport, similar to the liquid film in *Sarracenia*. As shown in Figure 1a,b, the micro/

nanostructured porous membrane is prepared by grafting polypyrrole (PPy) doped with β -naphthalenesulfonic acid (NSA) (in terms as PPy(NSA)) onto the meshed titanium (Figure S1). The prepared membrane performed excellent

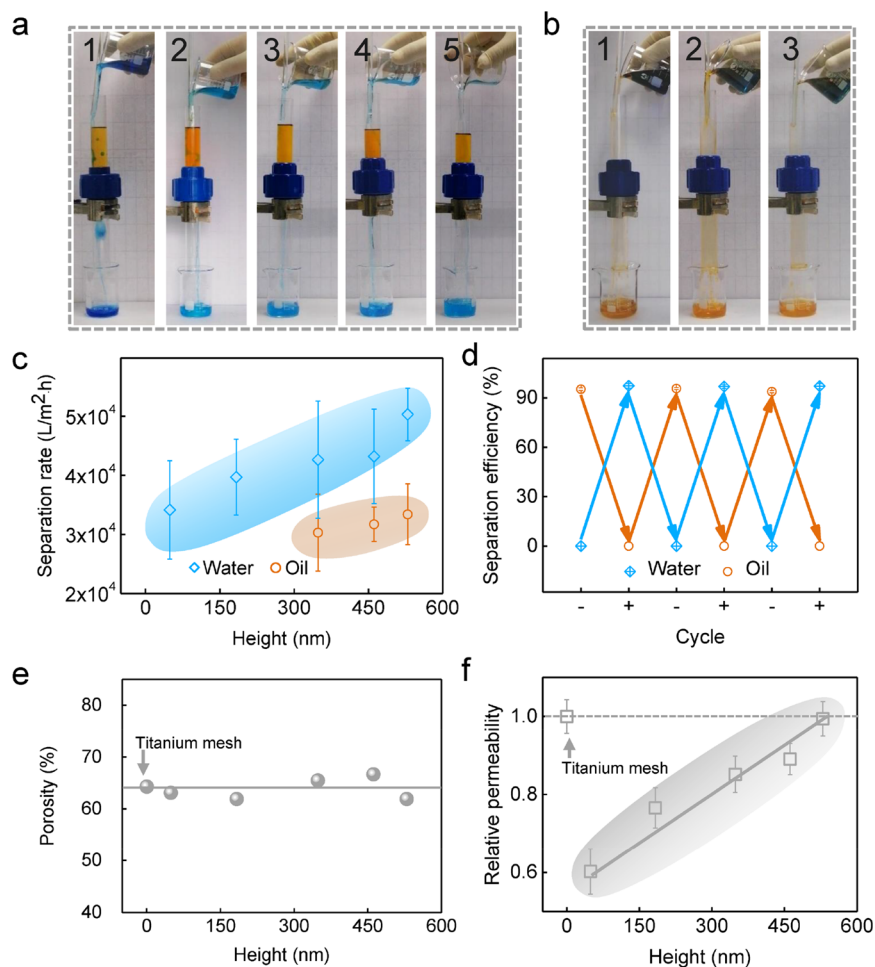


Figure 3. Ultrafast selective oil/water separation of the micro/nanostructured functional membrane. The photographs are of the oil/water separation of the oxidative membrane (a) with nanotip heights of 49, 183, 348, 461, and 529 nm and of the reductive membrane (b) with 348, 461, and 529 nm nanotip heights. The interval after the oil and water mixture is poured into the glass tube is 5 s for the oxidative membrane and 8 s for the reductive membrane. (c) The separation rate increases with the height of the nanotips. (d) The reversible smart oil/water separation through the transition of the reduction/oxidization (\mp) state of the membrane is shown. The porosity (e) and permeability (f) of the titanium mesh and membrane vary with the nanotip array height.

reversible electrochemical properties, which was evidenced by the cyclic voltammety curves (Figure S2). After the electro exchange along with the polymer (Figure S3), the wettability of the surface switches and the functional mesh could be applied as a separation membrane, as shown in Figure 1c. A typical structure of the membrane was presented in Figure 1d–f. The titanium mesh was constructed with microsized fibers, and the nanotips were perpendicular to the fiber. To systematically study the wettability properties and separation behavior, we constructed a series of porous membranes with tunable heights of the nanotips (from 49 ± 6 to 529 ± 77 nm) by controlling the growth time (Figure 1g, Figure 2a, and Figure S4).

For both chemical composition and surface roughness play pivotal roles in the wettability,^{22–24} the effects of chemical state and geometric structure on water wettability of the micro/nanostructured membrane were investigated here as shown in Figure 2 and Figure S5. The water contact angles (WCAs) (in air) could be changed from 137° to 0° (from superhydrophobic to superhydrophilic) with different times of redox potential. Furthermore, the WCAs (in air) of the membrane could be precisely and reversibly modulated as well (Figure S6 and S7). The WCAs of the flat membrane changed

little during the redox process (Figure S8) since there was no roughness factor. With the height of nanotips up to 348 nm, the membrane shows superwettability switch behavior (contact angles is more than 150° or less than 30°), and this trend is consistent with that of the microscale arrays surface.²⁵ This behavior was attributed to the stable three-phase contact line (i.e., the gas phase between the nanotips, liquid, and nanotips' solid phase).²⁵

The electric-responsive wettability transition of the membrane implied that this mesh could be applied to control oil/water separation (Figure 3). As the video and figures demonstrated, the oil/water mixture could ultrafast selectively flow through the micro/nanostructured membrane (Figure 3a,b and videos 1 and 2). This reversible separation efficiency is up to 97.3% in many runs (Figure 3d). Significantly, the separation speed of the membrane raised along with the height of nanotips. The oxidative membrane with nanotip height of 529 nm exhibited a promising water flux of $50326 \text{ L} \cdot \text{m}^{-2} \cdot \text{h}^{-1}$. Furthermore, the reductive one performed an excellent oil flux of $33401 \text{ L} \cdot \text{m}^{-2} \cdot \text{h}^{-1}$. To our best knowledge, this is currently the highest separation rate in selective oil/water separation.^{26–28} Moreover, the oil/water separation

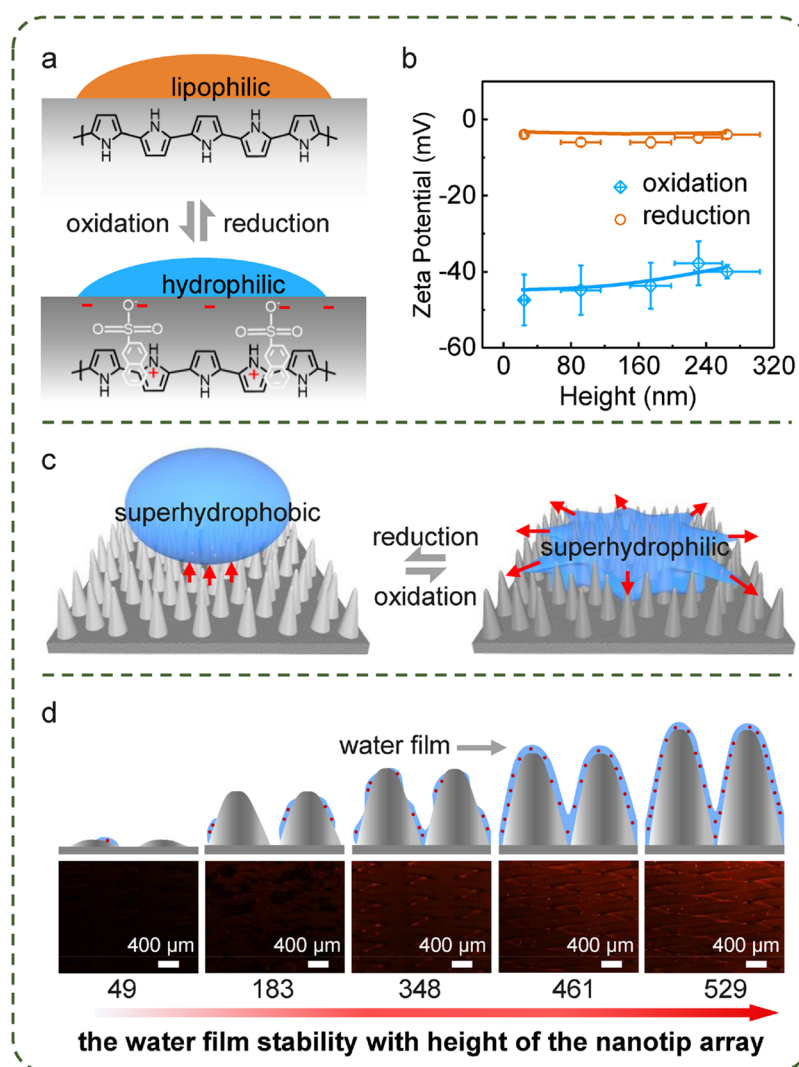


Figure 4. Schematic illustration of the reversible superwetting transition and ultrafast water transport on nanotip arrays. (a) The binary state surface (protonation/deprotonation) governs the wettability transition between hydrophilic and lipophilic. (b) The relationship between the ζ potential and nanotip height demonstrates that the ζ potential is related to the chemical state, regardless of height. (c) The reversible wettability switching process between the oxidized and reduced state of PPy is shown. The red arrows show the spreading direction of the water droplets. (d) The water film stability varies with the height of the nanotip array.

properties of the membrane were stable in harsh conditions and after long-term storage (Figures S10 and S11).

To further investigate the mechanism of the separation process, the porosity and permeability of the titanium mesh and the membrane with nanotip array were both demonstrated, as shown in Figure 3e,f. The porosity of the modified membrane was almost the same with the bare titanium mesh (Figure 3e), for the polymer brush is within nanoscale and the pore size of titanium mesh is $45 \mu\text{m}$. The permeability of the membrane decreased sharply after being modified the polymer brush. Surprisingly, the permeability of the membrane directly increases with the height of the nanotip, which is ultimately almost the same with the microscaled titanium mesh (Figure 3f).

We consider that the movement of the doping ion NSA into/out of the nanotip dominates wettability exchange (Figure 4a) for no physical structure change was observed during the redox process (Figure S9). In the reduced state, the PPy membrane performed hydrophobic/oleophilic as the doping ion travels outward the polymer main chain. While

the surfactant NSA enters into the polymer, the oxidized membrane was negatively charged testified by the ζ potential (Figure 4b). Immersing in the water, the sulfonation acid group tended into water, and the membrane behaves hydrophilic/oleophobic (Figure 4a). So the WCA could also be regulated with different times of redox potential (Figure S6). Combining the nanoscaled nanotips with chemistry,^{25,29} The superwettability switch between the Cassie and Wenzel state is realized in this system (Figure 4c).

As discussed above, the height of the polymer brush affects the permeability. This trend is the same with contact angles, as shown in Figure 2, which suggested the polymer brush plays a vital role in both wettability states and dynamic fluidic flow. Due to the Laplace pressure difference,^{30–34} the water droplet spreads along the tips, and the Laplace pressure difference (F_L) can be determined by $F_L = \pi\gamma R_b^2 \left(\frac{1}{R_a} - \frac{1}{R_b} \right)$ (R_a and R_b are the local radii of nanotips at the two opposite sides of water droplets) (Figure S12).

The wetting film would have a significant impact on the liquid transport, and the stability of the film depends on the height of the nanotips, as shown in Figure 4d. When the height is less than 348 nm, the WCA under oil is about a few tens of degrees, and the surface has not reached the superhydrophilic state (Figure 2c). In this case, the interaction between the surface and the wetting film is weak, and the wetting film appears only in patches, which could be driven away easily by the flow. The exposure of the surface roughness enhanced the friction to the flow, leading to the reduction of the permeability compared to the bare titanium mesh. When the nanotip height increases above 348 nm, the surface becomes superhydrophilic. The wetting liquid is then stabilized by the nearby nanotips, as shown by the following experiments. After being immersed in the rhodamine B solution, the functional membrane was rinsed by static immersion (Figure 4d) or dynamic rinsing (Figure S13). The fluorescence signal intensity increased with the height of nanotips, which demonstrated that the nanotips could enhance the water film stability. This continuous wetting film acts as a lubrication layer, leading to an increase of the permeability.

Overall, we have developed a novel weak electric field response micro/nanostructured porous membrane with conducting polymer nanotip arrays that performed reversibly superwetting switch and ultrafast selective oil/water separation. Under the synergistic effect of the chemical state and physical structure of nanotips, we can precisely control the wettability and realize the superwetting transition. The experimental observation showed that the separation speed was enhanced more than 1.5 times by increasing the nanotip length. The nanotip provided a stable environment of a thin and continuous water film, which would benefit the ultrafast water transport. This work not only can promote further understanding of the inner mechanism of the transform of surface wettability but also can develop a functional membrane for industrial applications in stimulating responsive oil–water separation. Furthermore, we believe this design could be applied in a complex environment, including bacterial and oil-contaminated wastewater treatment, and blood lipid filtration.

■ ASSOCIATED CONTENT

Supporting Information

The Supporting Information is available free of charge at <https://pubs.acs.org/doi/10.1021/acs.nanolett.0c00911>.

Experimental procedure, FE-SEM images, CV curves, XPS spectra, potential vs time curve, contact angles vs time, reversible wettability transition, separation efficiency, schematic of water droplet spreading, and hydrophilic and hydrophobic formation and stability of water film (PDF)

Oil/water separation for the oxidative membrane with a nanotip height of 348 nm (MP4)

Oil/water separation for the reductive membrane with a nanotip height of 348 nm (MP4)

■ AUTHOR INFORMATION

Corresponding Authors

Chengyun Ning – School of Material Science and Engineering and National Engineering Research Center for Tissue Restoration and Reconstruction, South China University of Technology, Guangzhou 510641, P. R. China; orcid.org/0000-0003-3293-4716; Email: imcyning@scut.edu.cn

Yahong Zhou – CAS Key Laboratory of Bio-inspired Materials and Interfacial Science, Technical Institute of Physics and Chemistry, Chinese Academy of Sciences, Beijing 100190, P. R. China; Email: zhouyh@mail.ipc.ac.cn

Authors

Zhengao Wang – School of Material Science and Engineering and National Engineering Research Center for Tissue Restoration and Reconstruction, South China University of Technology, Guangzhou 510641, P. R. China

Peng Yu – School of Material Science and Engineering and National Engineering Research Center for Tissue Restoration and Reconstruction, South China University of Technology, Guangzhou 510641, P. R. China; orcid.org/0000-0002-2253-7373

Jiajia Zhou – Center of Soft Matter Physics and Its Application, Beihang University, Beijing 100191, P. R. China; orcid.org/0000-0002-2258-6757

Jingwen Liao – Guangzhou Institute of Advanced Technology, Chinese Academy of Sciences, Guangzhou 511458, P. R. China

Lei Zhou – School of Material Science and Engineering, South China University of Technology, Guangzhou 510641, P. R. China

Heying Ran – School of Material Science and Engineering, South China University of Technology, Guangzhou 510641, P. R. China

Jingxia Zhai – School of Material Science and Engineering, South China University of Technology, Guangzhou 510641, P. R. China

Jun Xing – School of Material Science and Engineering, South China University of Technology, Guangzhou 510641, P. R. China

Guoxin Tan – Institute of Chemical Engineering and Light Industry, Guangdong University of Technology, Guangzhou 510006, P. R. China; orcid.org/0000-0001-8647-639X

Zhengen Zhou – School of Material Science and Engineering, South China University of Technology, Guangzhou 510641, P. R. China

Yangfan Li – School of Material Science and Engineering, South China University of Technology, Guangzhou 510641, P. R. China

Complete contact information is available at:

<https://pubs.acs.org/doi/10.1021/acs.nanolett.0c00911>

Author Contributions

[†]Z.W. and P.Y. contributed equally. C.N. and Y.Z. conceived the idea. Z.W., J.L., H.R., J.Z., J.X., G.T., Z.Z., and Y.L. participated in the synthesis of the functional membrane and TEM, SEM, ζ potential characterization, and oil/water separation. Z.W. characterized the water film. J.Z. and Y.Z. conducted the mechanism of oil/water separation. C.N. and Y.Z. supervised the project. Z.W. and Y.Z. wrote the manuscript.

Notes

The authors declare no competing financial interest.

■ ACKNOWLEDGMENTS

This work is financially supported by the National Key R&D Program of China (Nos. 2018YFC1105304 and 2018YFC1105301), the National Natural Science Foundation of China (Nos. 51932002, 31771080, 51702104, 51903087, 51703037, and 51772106), the Science and Technology

Innovation Project of Foshan (No. 2018IT100101), and the Natural Science Foundation of Guangdong Province (No. 2016A030308014).

REFERENCES

- (1) Feng, L.; Zhang, Z.; Mai, Z.; Ma, Y.; Liu, B.; Jiang, L.; Zhu, D. A super-hydrophobic and super-oleophilic coating mesh film for the separation of oil and water. *Angew. Chem., Int. Ed.* **2004**, *43*, 2012–2014.
- (2) Liang, B.; Wang, H.; Shi, X. H.; Shen, B. Y.; He, X.; Ghazi, Z. A.; Khan, N. A.; Sin, H.; Khattak, A. M.; Li, L. S.; Tang, Z. Y. Microporous membranes comprising conjugated polymers with rigid backbones enable ultrafast organic-solvent nanofiltration. *Nat. Chem.* **2018**, *10* (9), 961–967.
- (3) Wang, B.; Liang, W.; Guo, Z.; Liu, W. Biomimetic super-lyophobic and super-lyophilic materials applied for oil/water separation: a new strategy beyond nature. *Chem. Soc. Rev.* **2015**, *44*, 336–61.
- (4) Wang, L.; Zhao, Y.; Tian, Y.; Jiang, L. A General Strategy for the Separation of Immiscible Organic Liquids by Manipulating the Surface Tensions of Nanofibrous Membranes. *Angew. Chem., Int. Ed.* **2015**, *54*, 14732–7.
- (5) Zhang, J.; Seeger, S. Polyester materials with superwetting silicone nanofilaments for oil/water separation and selective oil absorption. *Adv. Funct. Mater.* **2011**, *21*, 4699–4704.
- (6) Xue, Z.; Cao, Y.; Liu, N.; Feng, L.; Jiang, L. Special wettable materials for oil/water separation. *J. Mater. Chem. A* **2014**, *2*, 2445–2460.
- (7) Guo, F.; Guo, Z. Inspired smart materials with external stimuli responsive wettability: a review. *RSC Adv.* **2016**, *6*, 36623–36641.
- (8) Zhang, S.; Zhang, J.; Fang, W.; Zhang, Y.; Wang, Q.; Jin, J. Ultralarge single-layer porous protein nanosheet for precise nanosize separation. *Nano Lett.* **2018**, *18*, 6563–6569.
- (9) Chen, C.; Weng, D.; Mahmood, A.; Chen, S.; Wang, J. Separation Mechanism and Construction of Surfaces with Special Wettability for Oil/Water Separation. *ACS Appl. Mater. Interfaces* **2019**, *11*, 11006–11027.
- (10) Zhang, D.; Cheng, Z.; Kang, H.; Yu, J.; Liu, Y.; Jiang, L. A smart superwetting surface with responsivity in both surface chemistry and microstructure. *Angew. Chem., Int. Ed.* **2018**, *57*, 3701–3705.
- (11) Liu, M.; Wang, S.; Jiang, L. Nature-inspired superwettability systems. *Nat. Rev. Mater.* **2017**, *2*, 17036.
- (12) Si, Y.; Guo, Z. Superwetting materials of oil-water emulsion separation. *Chem. Lett.* **2015**, *44*, 874–883.
- (13) Yang, Y.; Li, X.; Zheng, X.; Chen, Z.; Zhou, Q.; Chen, Y. 3D-Printed Biomimetic Super-Hydrophobic Structure for Microdroplet Manipulation and Oil/Water Separation. *Adv. Mater.* **2018**, *30*, 1704912.
- (14) Fu, Q.; Ansari, F.; Zhou, Q.; Berglund, L. A. Wood nanotechnology for strong, mesoporous, and hydrophobic biocomposites for selective separation of oil/water mixtures. *ACS Nano* **2018**, *12*, 2222–2230.
- (15) Chu, Z.; Feng, Y.; Seeger, S. Oil/water separation with selective superantiwetting/superwetting surface materials. *Angew. Chem., Int. Ed.* **2015**, *54* (8), 2328–38.
- (16) Ma, Q.; Cheng, H.; Fane, A. G.; Wang, R.; Zhang, H. Recent development of advanced materials with special wettability for selective oil/water separation. *Small* **2016**, *12*, 2186–2202.
- (17) Freger, V. Outperforming nature's membranes. *Science* **2015**, *348*, 1317–1318.
- (18) Shi, Z.; Zhang, W.; Zhang, F.; Liu, X.; Wang, D.; Jin, J.; Jiang, L. Ultrafast Separation of Emulsified Oil/Water Mixtures by Ultrathin Free-Standing Single-Walled Carbon Nanotube Network Films. *Adv. Mater.* **2013**, *25*, 2422–2427.
- (19) Zhang, X.; Li, Z.; Liu, K.; Jiang, L. Bioinspired multifunctional foam with self-cleaning and oil/water separation. *Adv. Funct. Mater.* **2013**, *23*, 2881–2886.
- (20) Zeng, X.; Qian, L.; Yuan, X.; Zhou, C.; Li, Z.; Cheng, J.; Xu, S.; Wang, S.; Pi, P.; Wen, X. Inspired by Stenocara Beetles: From Water Collection to High-Efficiency Water-in-Oil Emulsion Separation. *ACS Nano* **2017**, *11*, 760–769.
- (21) Chen, H.; Ran, T.; Gan, Y.; Zhou, J.; Zhang, Y.; Zhang, L.; Zhang, D.; Jiang, L. Ultrafast water harvesting and transport in hierarchical microchannels. *Nat. Mater.* **2018**, *17*, 935–942.
- (22) Wang, Y.; Gong, X. Special oleophobic and hydrophilic surfaces: approaches, mechanisms, and applications. *J. Mater. Chem. A* **2017**, *5*, 3759–3773.
- (23) Firkowska-Boden, I.; Zhang, X.; Jandt, K. D. Controlling protein adsorption through nanostructured polymeric surfaces. *Adv. Healthcare Mater.* **2018**, *7*, 1700995.
- (24) Li, T.; Liu, F.; Zhang, S.; Lin, H.; Wang, J.; Tang, C. Y. Janus Polyvinylidene Fluoride Membrane with Extremely Opposite Wetting Surfaces via One Single-Step Unidirectional Segregation Strategy. *ACS Appl. Mater. Interfaces* **2018**, *10*, 24947–24954.
- (25) Oner, D.; McCarthy, T. J. Ultrahydrophobic Surfaces. Effects of Topography Length Scales on Wettability. *Langmuir* **2000**, *16*, 7777–7782.
- (26) Raza, A.; Ding, B.; Zainab, G.; El-Newehy, M.; Al-Deyab, S. S.; Yu, J. In situ cross-linked superwetting nanofibrous membranes for ultrafast oil-water separation. *J. Mater. Chem. A* **2014**, *2*, 10137–10145.
- (27) Che, H.; Huo, M.; Peng, L.; Fang, T.; Liu, N.; Feng, L.; Wei, Y.; Yuan, J. CO₂-Responsive Nanofibrous Membranes with Switchable Oil/Water Wettability. *Angew. Chem., Int. Ed.* **2015**, *54*, 8934–8.
- (28) Wang, K.; Han, D. S.; Yiming, W.; Ahzi, S.; Abdel-Wahab, A.; Liu, Z. A windable and stretchable three-dimensional all-inorganic membrane for efficient oil/water separation. *Sci. Rep.* **2017**, *7*, 16081.
- (29) Koishi, T.; Yasuoka, K.; Fujikawa, S.; Ebisuzaki, T.; Zeng, X. C. Coexistence and transition between Cassie and Wenzel state on pillared hydrophobic surface. *Proc. Natl. Acad. Sci. U. S. A.* **2009**, *106*, 8435–8440.
- (30) Quéré, D. Thin films flowing on vertical fibers. *Europhys. Lett.* **1990**, *13*, 721.
- (31) Washburn, E. W. The Dynamics of Capillary Flow. *Phys. Rev.* **1921**, *17*, 273–283.
- (32) Ju, J.; Bai, H.; Zheng, Y.; Zhao, T.; Fang, R.; Jiang, L. A multi-structural and multi-functional integrated fog collection system in cactus. *Nat. Commun.* **2012**, *3*, 1247.
- (33) Lorenceau, E.; Quere, D. Drops on a conical wire. *J. Fluid Mech.* **1999**, *510*, 29–45.
- (34) Li, K.; Ju, J.; Xue, Z.; Ma, J.; Feng, L.; Gao, S.; Jiang, L. Structured cone arrays for continuous and effective collection of micron-sized oil droplets from water. *Nat. Commun.* **2013**, *4*, 2276.

Supporting Information

Ultrafast and On-demanded Oil/Water Separation Membrane System Based on Conducting Polymer Nanotip Arrays

Zhengao Wang, Peng Yu, Jiajia Zhou, Jingwen Liao, Lei Zhou, Heying Ran, Jingxia Zhai, Jun Xing, Guoxin Tan, Zhengnan Zhou, Yangfan Li, Chengyun Ning and Yahong Zhou**

Content

- (1) Micro/nano-structured porous membrane fabrication**
- (2) Potential-induced reversible switch in superwettability**
- (3) Ultrafast and controllable Oil/water separation through electric-field stimulation**
- (4) Characterization of micrograph and chemical composition**
- (5) Supplementary Figures**
- (6) Supplementary Video Legends**

Materials

Pyrrrole (Py), Hydrofluoric acid (HF), nitric acid (HNO₃), β-naphthalenesulfonic acid (NSA), Sudan II, methylene blue and rhodamine B were purchased from Shanghai Aladdin biochemical Technology Co. Ltd., Shanghai, China. The titanium meshes (320 meshes) were purchased from Anping Hongyun Metal Products Co. Ltd., Hengshui, China. The thickness of the Ti mesh is 600 μm. The pore size of the Ti mesh is 45 μm. The fiber diameter of the Ti mesh is 180 (warp) × 220 (weft) μm². Hexane was purchased from Shanghai Macklin Biochemical Co. Ltd., Shanghai, China. Hydrochloric acid (HCl) were purchased from Guangzhou Chemical Reagent Factory, Guangzhou, China.

Micro/nano-structured porous membrane fabrication

The titanium meshes were ultrasonically cleaned in a mixture solution of HF, HNO₃, and HO₂ (volume ratio = 1:1:100) for 30 min, and then ultrasonically cleaned in acetone, methanol and distilled water for 20 min. The dry titanium meshes were sandblasted with corundum 80 mesh. The processed titanium meshes were ultrasonically cleaned in acetone, methanol, and distilled water for 20 min. The polypyrrole nanotips were grafted on the titanium mesh through electrochemical polymerization. In detail, the smooth PPy films were first deposited on titanium mesh at 0.9 V (vs. Ag/AgCl) for 60 s. The electrolyte was 0.25 M HCl and 0.2 M Py solution. Second, PPy nanotips were grafted galvanostatically on smooth PPy coated titanium membrane at 3.6 mA/cm² for 5,

15, 30, 45, or 60 min, respectively. The height of nanotips could be tuned by controlling the deposition time. The electrolyte was a phosphate buffer solution (PBS, 0.5 M, pH 6.8) containing 0.2 M Py and 0.01 M β -naphthalenesulfonic acid (NSA).

Potential-induced reversible switch in superwettability

To determine the redox potentials of micro/nano-structured porous membrane, cyclic voltammetry (CV) was measured in an electrochemical system made of an electrolyte (PBS, 0.5 M, pH 6.8), porous membrane as a working electrode, platinum electrode as a counter electrode, and Ag/AgCl electrode as a reference electrode. The CV curves of the porous membrane were recorded by applying a scanning potential from 0.5 V to -1.0 V at a scan rate of 5 mV/s. The resultant CV curves of the membrane demonstrated that the reduction and oxidation potentials were -0.55 V and -0.34 V, respectively. Then we used the electrochemical station to apply negative potential (-0.80 V) to trigger reduction reactions of the membrane (working electrode) for 10 min, and the reductive membrane (-) was obtained. The reductive membrane (-) was then taken out of the station and dried in air, followed by the measurement of water contact angle (WCA) of a 2 μ L water droplet on the membrane by surface contact angle analyzer at ambient temperature. Simultaneously, the under-oil WCA and under-water the oil contact angle (OCA) was determined. Then the reductive membrane was dried and placed into the electrochemical station again and a positive potential (+ 0.50 V) was applied to trigger the oxidation reactions of membrane for 10 min, and the oxidative membrane (+) was obtained.

Contact Angles test: The WCA in air, under-oil, and under-water OCA of oxidative (+) and reductive (-) membrane was determined. This redox reaction is repeated many times. What's more, in order to explore the effect of the time of

applying the external field on the WCA, the WCA was characterized after the nanotips-grafted membrane with a growth time of 30 min was reduced or oxidized for 1, 2, 4, 8, 12, 16 min, respectively.

Ultrafast and controllable Oil/water separation through electric-field stimulation

The oxidative membrane was sandwiched between two glass tubes coupled together with a simple commercial water pipe joint. The inner diameter and the length of glass tubes is 1.8 cm and 10.0 cm, respectively. Then a mixture of 20 mL cyclohexane (dyed with Sudan II) and 20 mL water (dyed with methylene blue) was poured into the upper tube. The separation process was only driven by gravity without an external force. After being used to separate oil/water, the oxidative membrane was washed. The oxidative membrane was reduced in an electrochemical cell, and the reductive membrane was prepared. The dry reductive membrane was used to separate oil/water mixture. The parameters of the oxidation reaction and reduction reaction are consistent with one of the contact angle test parts. The oil/water separation efficiency was defined to be the percentage between the weight of liquid after separation and that of the original liquid before separation. The water and oil fluxes of the mesh were calculated based on the flow weight per unit time from the valid area of the membranes.

Characterization of micrograph and chemical composition

Field emission scanning electron microscopy (FE-SEM, ZEISS Merlin, Germany) and transmission electron microscope (TEM, JEM-1400 PLUS, Japan) were used to characterize surface topography of sample. X-ray photoelectron spectroscopy (XPS, Kratos Axis Ultra DLD, Britain) was used to analyze the chemical composition of the sample. An electrochemical station (Zennium Zahner, Germany) was used to measure cyclic voltammetry (CV) and Polarization curve. Contact angle meter (KRUSS DSA25, German) was applied to character the WCA in air and under oil and OCA under water.

Supplementary Figures

FE-SEM images

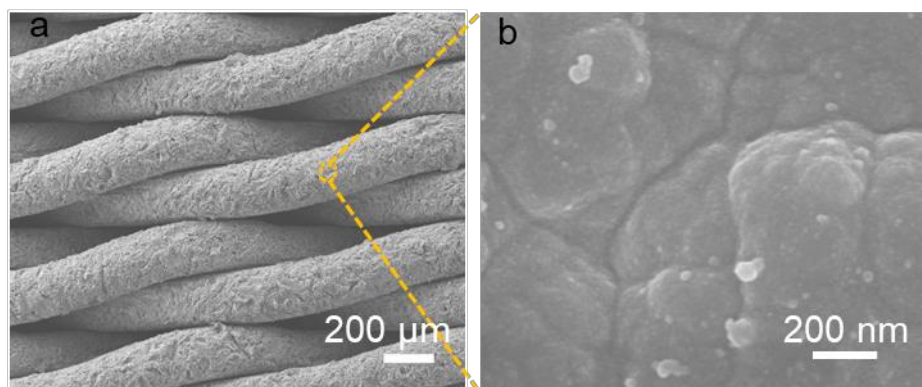


Figure S1. The field emission scanning electron microscopy (FE-SEM) of smooth PPy films coated on the titanium meshes. The smooth PPy films were first deposited on the titanium meshes, which served as the active sites for formation of PPy nanotips.^[1]

CV curves

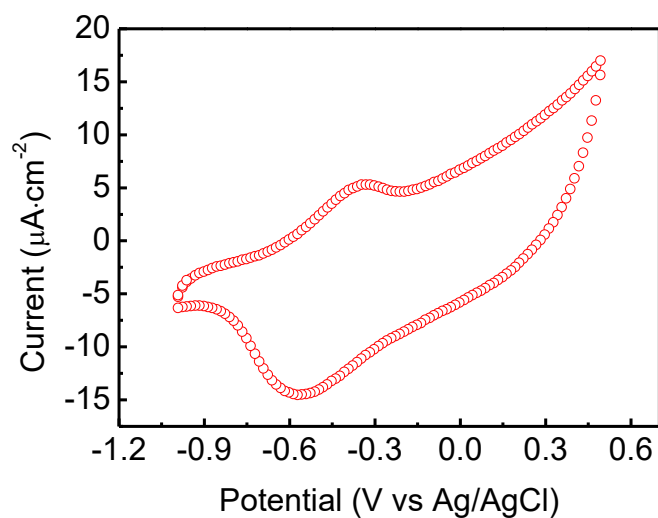


Figure S2. Cyclic voltammetry (CV) curve of PPy(NSA) nanotip arrays onto the titanium mesh. The redox reversibility of the as-obtained Ti-NTPPy membrane was evidenced by the good x axis symmetry of its cyclic voltammetry curves, which demonstrated that an oxidation peak at -0.34 V (vs. Ag/AgCl) and a reduction peak at -0.55V (vs. Ag/AgCl). Therefore, + 0.5 V/ - 0.8 V was selected as oxidation/reduction switch potentials to offer a weak wild electric field and the reduction state (Ti-reNTPPy, -) and oxidation state (Ti-oxNTPPy, +) of Ti-NTPPy meshes were obtained, respectively.

XPS characterization

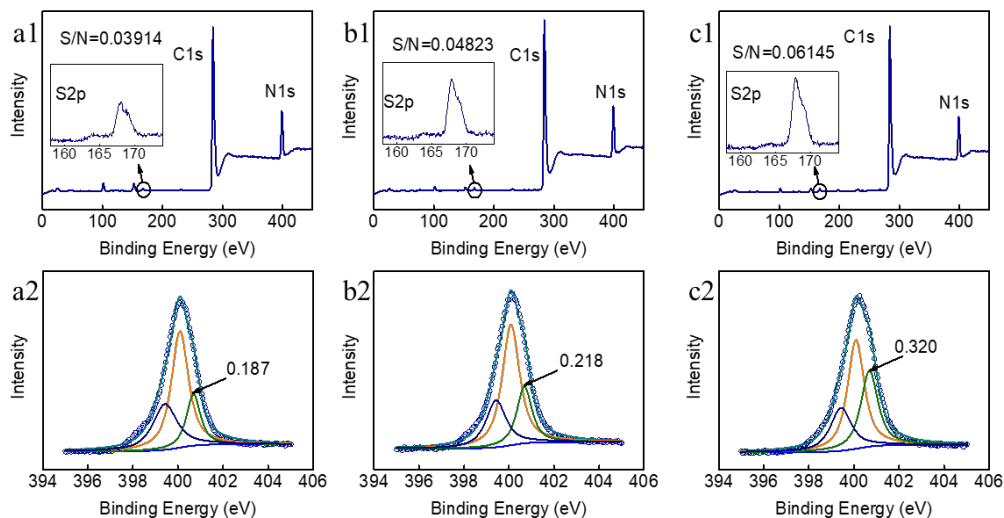


Figure S3. X-ray photoelectron spectroscopy (XPS) of PPy(NSA) nanotip arrays in reductive (a1, a2), original (b1, b2) and oxidative (c1, c2) state, respectively. According to the XPS spectra, the S/N of Ti-reNTPPy and Ti-oxPPy were 0.039 and 0.061, respectively, which demonstrated that the ratio of NSA dopant to pyrrole monomer increased from 0.039 to 0.061 after Ti-reNTPPy being oxidized. And the protonated nitrogen content (N^+/N) of Ti-oxNTPPy and Ti-reNTPPy are 0.320 and 0.187, respectively. Therefore, when our nanotips PPy was oxidized under a positive potential of +0.5 V, it was converted to a cationic radical, or polaron, and the counter ion was doped in the PPy chain.^[2]

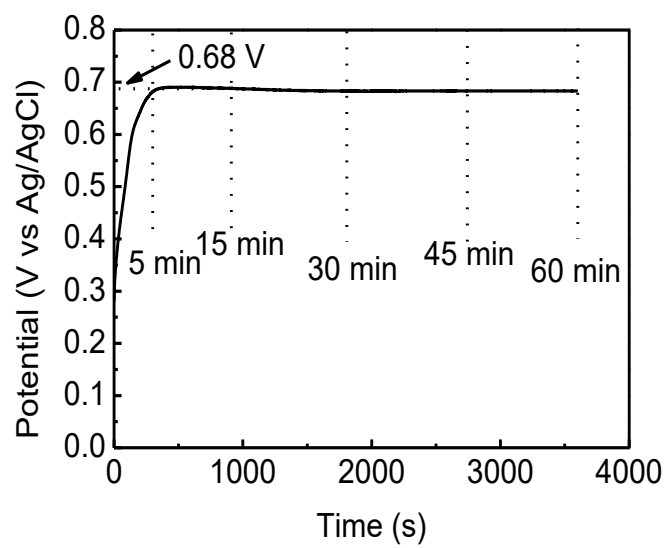


Figure S4. The potential vs. time curve when the nanotips grew on the titanium mesh.

The effect of NSA doping degree on the structure of PPy and the wettability switch

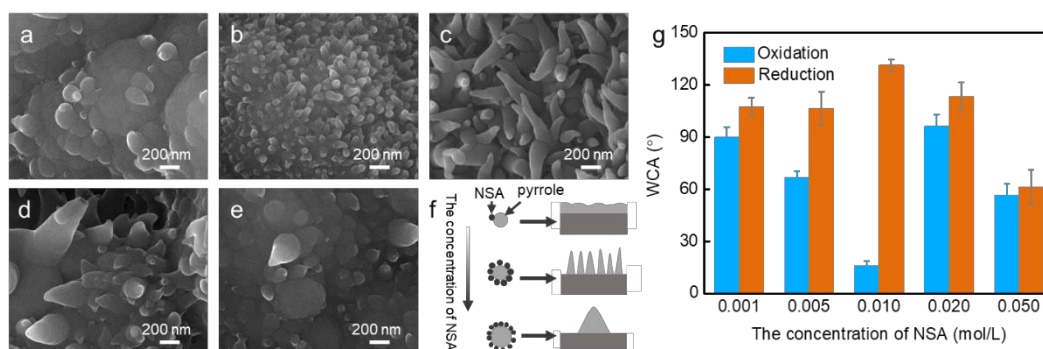


Figure S5. The effect of NSA doping degree on the topography and switchable wettability. (a-e) SEM images of nanostructured PPy(NSA) obtained in PBS containing 0.001m (a), 0.005 (b) 0.010m (c), and 0.020m (d), 0.50 (e) of NSA. (f) the schematic of the concentration of NSA controls the nanostructure. (g) the concentration of NSA controls the switchable wettability. The SEM showed that the doping concentration (0.001, 0.005, 0.010, 0.020, 0.050 M) determined the macro/nano-structure of polypyrrole. When the concentration of NSA was increased from 0.001 M to 0.010 M, and finally to 0.050 M, the PPy evolved from random nanostructure to dense nanotips to sparse large-sized nanotips. We believed that the NSA doping act as a surfactant to fabricate the nanotip. When the concentration of NSA is too low to stabilize the pyrrole nanomicelle, the pyrrole fails to aggregate along a fixed direction, which results in the random nanostructure. When the concentration of the NSA increased to an appropriate one, the stable pyrrole nanomicelle forms and polymerizes along the direction perpendicular to the substrates. This would lead to the nanotips. Furthermore, when the concentration of NSA continues to increase, the nanomicelle becomes

larger, and sparse large-sized nanotips form. Therefore, the doping degree determines the amplitude of the wettability switch through controlling the chemical composition and the structure of polypyrrole.

CAs varied with time of redox potential

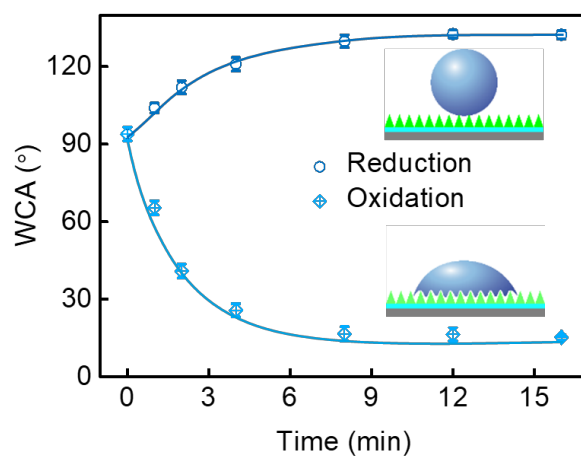


Figure S6. The contact angles (in air) of the PPy(NSA) nanotip arrays grafted membrane could be continuous/precisely modulated with different time of redox potential. The height of nanotips are about 170 nm. What's more, the WCA (in air) of the membrane could be continuous/precisely modulated with different time of redox potential (Figure S4). Applied with 0.5 V for 16min, the WCA of PPy (NSA) varied from 93.9° to 15.2°. And if -0.8 V, the WCA gradually increased to 132.3°.

Reversible wettability transition

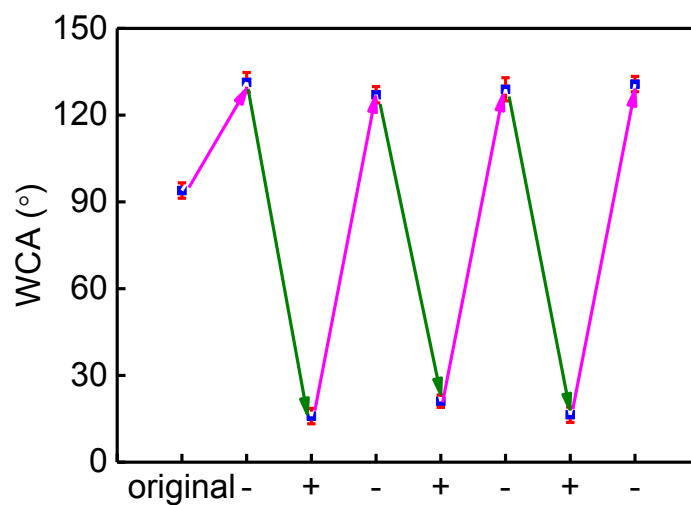


Figure S7. Reversible wettability transition on the nanotip arrays with height of 348 nm. The reductive membrane (-) was obtained by reducing the original functional membrane under negative potential (-0.80 V) for 10 min. The oxidative membrane (+) was obtained by oxidizing the reductive membrane under positive potential (+0.50 V) for 10 min.

CAs of control membranes

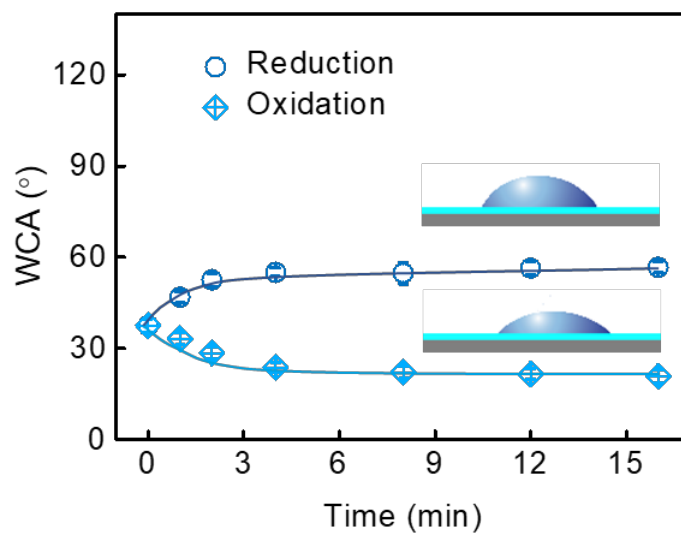


Figure S8. The contact angles (in air) of titanium mesh coated smooth PPy with different time of redox potential. After being oxidized for about 3 min, the contact angles (in air) of titanium mesh coated smooth PPy decreased from 37.5° to 20.9°. After being reduced for 2.5 min, the contact angles (in air) of titanium mesh coated smooth PPy increased from 37.5° to 20.9° to 56.4°.

FE-SEM images

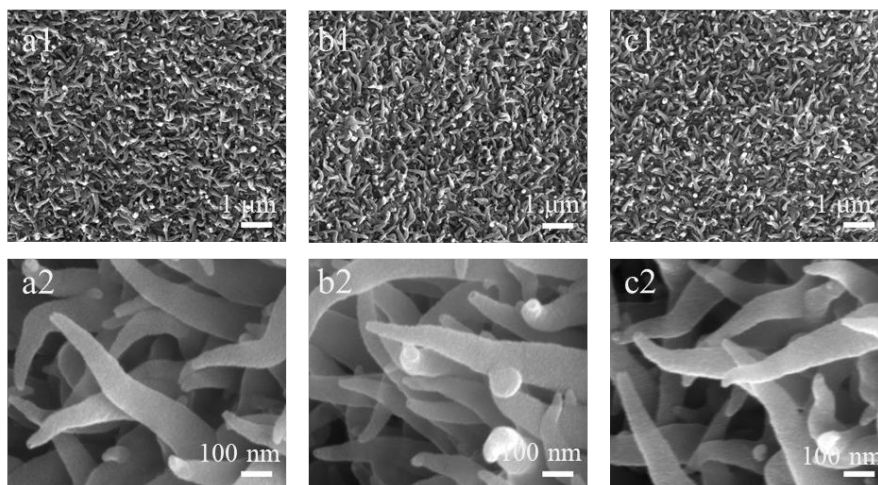


Figure S9. The field emission scanning electron microscopy (FE-SEM) of PPy(NSA) nanotip arrays grown for 60 min being in oxidation (a1, a2), original (b1, b2) and reduction (c1, c2) state. the morphology of PPy(NSA) nanotip arrays had change little under weak wild field.

The separation efficiency of various corrosive solutions

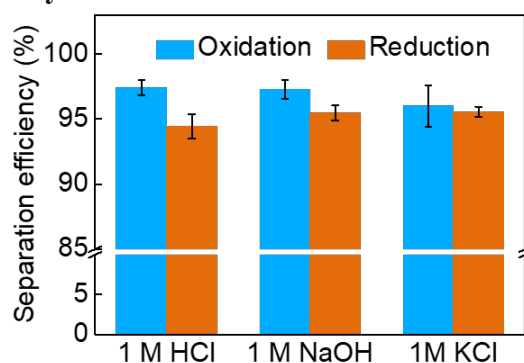


Figure S10. The separation efficiency of various corrosive solutions using the oxidative membrane (blue) and the separation efficiency of cyclohexane using the reductive membrane (yellow). The results showed that the functional membrane possessed excellent oil/water separation properties in harsh conditions. To examine the separation properties in harsh conditions, the oxidative and reductive membranes were used to separate the cyclohexane and various corrosive solutions mixture, including HCl/cyclohexane mixture, NaOH/cyclohexane, and mixture KCl/cyclohexane mixture. The separation efficiency of the as-prepared membranes was higher than 95% for cyclohexane/corrosive water mixtures, which proved the stable separation properties in harsh conditions.

The separation efficiency *versus* storage time

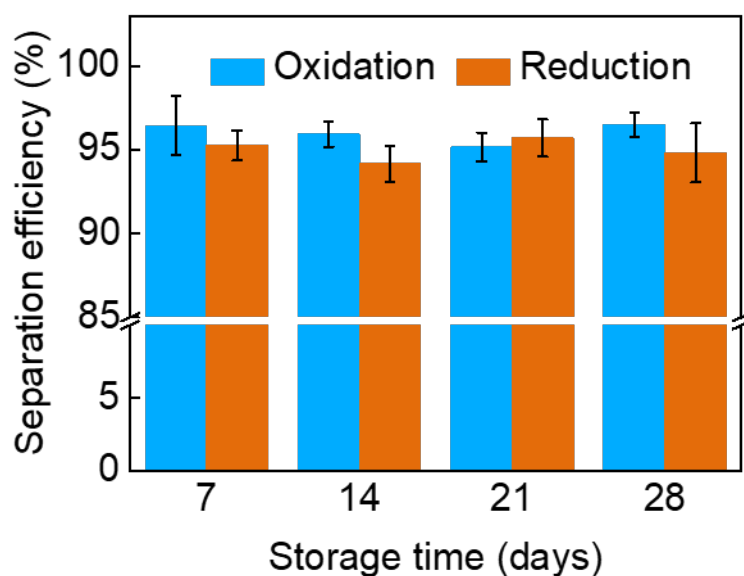


Figure S11. The separation efficiency *versus* storage time after the functional being stored in vacuum. The functional membrane possessed stable separation during 4 weeks of storage times in vacuum. After the electrical stimuli, the membranes were stored in a vacuum, and then were used to separate cyclohexane/water mixture. The separation efficiency *versus* storage time demonstrated that the separation meshes stayed almost unchanged during four weeks of storage times.

The water droplet spreading along the nanotips

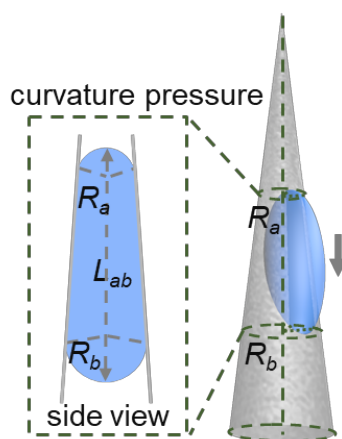


Figure S12. The schematic description of the water droplet spreading along the nanotips driven by the curvature pressure.

The water film

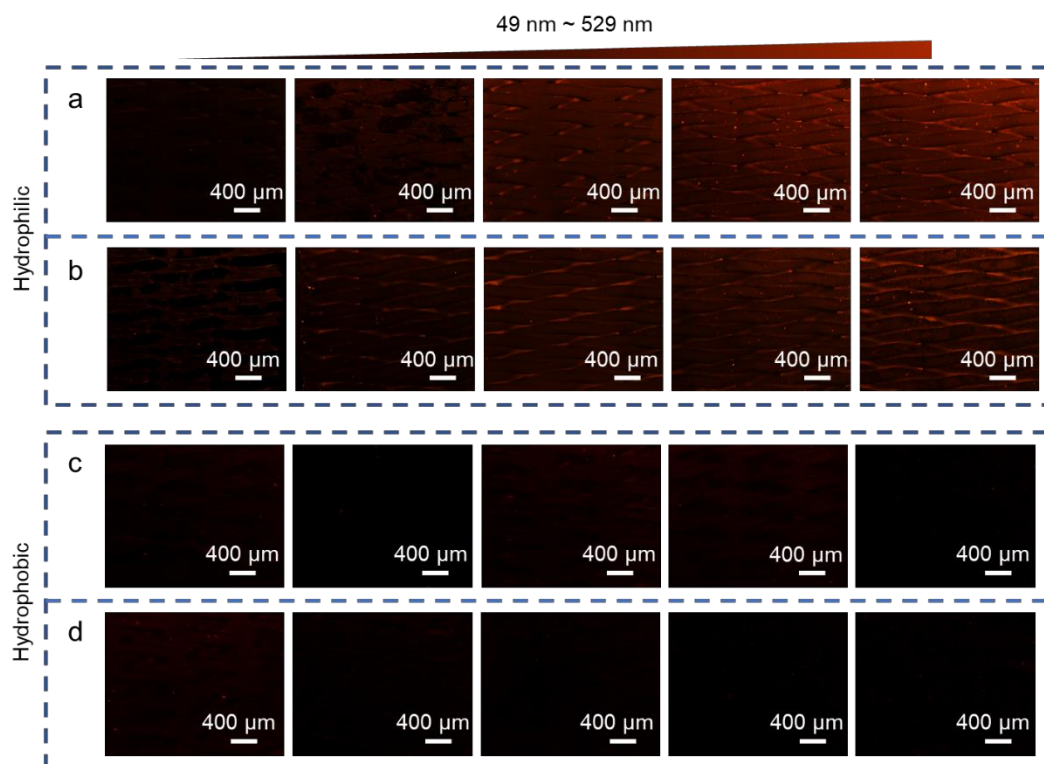


Figure S13. The formation and stability of water film on the micro/nano-structured membrane. (a) The oxidative micro/nano-structured immersed in the rhodamine B solution for 5 min and then immersed in the deionized water for 1 min. Finally, an upright fluorescence microscope was used to observe the water film. (b) After the membrane being immersed in the rhodamine B solution, 1 mL deionized water drops from the height of about 10 cm on the surface of the oxidative membrane. Then the water film on the membrane was observed. The water film disappeared on the surface of the reductive micro/nano-structured membrane after the membrane was dealt with static immersion (c) or dynamic rinsing (d).

Supplementary Video Legends

Supplementary Video 1. The oxidative membrane with nanotips height of 348 nm was applied to separate ultrafast water from oil/water mixture. As for the oxidative membrane, a mixture of cyclohexane (dyed by Sudan II) and water (dyed by methylene blue) with 50% v/v was poured into the upper glass tube. Oil was retained above the mesh. Meanwhile, water could quickly permeate through the mesh and dropped into the beaker due to superhydrophilic under oil and superoleophobic underwater surface.

Supplementary Video 2. The reductive membrane with nanotips height of 348 nm was applied to super-fast separate oil from oil/water mixture. As for the reductive membrane, a mixture of cyclohexane (dyed by Sudan II) and water (dyed by methylene blue) with 50% v/v was poured into the upper glass tube. Oil could ultrafast permeate through the functional membrane, but water could not.

[1] J. Liao, Y. Zhu, Z. Zhou, J. Chen, G. Tan, C. Ning, C. Mao, *Angew. Chem., Int. Ed. Engl.* 2014, 53, 13068.

[2] L. Xu, W. Chen, A. Mulchandani, Y. Yan, *Angew. Chem., Int. Ed. Engl.* 2005, 44, 6009.